Science and Technology of Welding and Joining

ISSN: 1362-1718 (Print) 1743-2936 (Online) Journal homepage: http://www.tandfonline.com/loi/ystw20

Laser welding/brazing of 5182 aluminium alloy to ZEK100 magnesium alloy using a nickel interlayer

Jin Yang, Zhishui Yu, Yulong Li, Hua Zhang & Norman Zhou

To cite this article: Jin Yang, Zhishui Yu, Yulong Li, Hua Zhang & Norman Zhou (2018): Laser welding/brazing of 5182 aluminium alloy to ZEK100 magnesium alloy using a nickel interlayer, Science and Technology of Welding and Joining, DOI: 10.1080/13621718.2018.1425182

To link to this article: https://doi.org/10.1080/13621718.2018.1425182

Published online: 19 Jan 2018.

SCIENCE AND TECHNOLOGY OF WELDING AND JOINING, 2018
https://doi.org/10.1080/13621718.2018.1425182

The Institute of Materials, Minerals and Mining

Taylor & Francis
Taylor & Francis Group

Laser welding/brazing of 5182 aluminium alloy to ZEK100 magnesium alloy using a nickel interlayer

Jin Yang [a], Zhishui Yu[a], Yulong Li[b], Hua Zhang[b] and Norman Zhou[c]

[a]School of Materials Engineering, Shanghai University of Engineering Science, Shanghai, People's Republic of China; [b]Key Lab of Robot and Welding Automation of Jiangxi Province, School of Mechanical and Electrical Engineering, Nanchang University, Nanchang, People's Republic of China; [c]Center for Advanced Materials Joining, University of Waterloo, Waterloo, Canada

ABSTRACT

Aluminium alloy and magnesium alloy were successfully joined by using laser welding/brazing technology via a nickel interlayer. Microstructure and mechanical properties of the dissimilar Al/Mg joints with and without a nickel interlayer were comparatively investigated. No joints were achieved without a nickel interlayer; after welding, specimens were separated without applying any force. By inserting a nickel interlayer, sound metallurgical bonding were obtained at the interfaces. Hence, the joint strength reached 410 N with the failure at Mg/Ni interface. The influence of Ni interlayer on the weld defect, microstructure and joint strength was studied, and the joint formation mechanism was also discussed.

ARTICLE HISTORY
Received 21 July 2017
Accepted 30 December 2017

KEYWORDS
Laser welding/brazing; aluminium alloy; magnesium alloy; nickel interlayer; intermetallic compounds; joint strength

Introduction

Sustainable growth in automotive industry will be increasingly contingent upon the development of energy-saving products that economically use and conserve resources while protecting the global environment through emission reductions. Employing lightweight materials such as Al and Mg alloys is an effective way to reduce emissions, since reducing vehicle weight can greatly lower fuel consumption [1–3]. Therefore, a reliable bonding between Al and Mg alloys is increasingly attracting the academic and industrial interest.

In spite of the wide interest, the application of Al/Mg dissimilar joint is still confined. This is because of the formation of brittle Mg/Al intermetallic compounds (IMCs) that impairs the mechanical performance of joints [4–6]. Thus, eliminating Mg/Al (IMCs) or improving their distribution state has become the key to realise an effective joining of Mg and Al alloys. To date, many joining technologies have been used to address this issue in Al/Mg joining. Solid-state welding is a promising method as the formation and growth of Al/Mg IMCs can be significantly limited by avoiding the melting of parent metals. Kou et al. [7] investigated the effect of material position, travel speed, and rotation speed on the microstructure and strength of friction stir butt welded Al/Mg joint. Chowdhury et al. [1] studied the influence of adhesive layer and joint configuration on the lap shear strength and fatigue behaviour of the friction spot welded Al/Mg joint. Panteli et al. [8] optimised the weldingconditions, heat generation, and the formation intermetallic reaction layer in Al/Mg ultrasonic spot welding. In another investigation of ultrasonic spot welding of Al to Mg, Patel et al. [9] observed a layer of brittle $Al_{12}M_{17}$ in the weld zone which facilitated the crack propagation before joint failure. However, the shape and size of solid-state-welded joints are extremely restricted, and therefore the joint application could be narrowed.

By virtue of high processing speed, high energy density and high flexibility, laser welding/brazing is promising for the joining of dissimilar materials. By utilising the great difference in melting points of parent metals, it allows the formation of a fusion welded joint at one side and a brazed joint at the other side. In this technology, a key step is to choose an appropriate interlayer, filler metal, coating or their combinations for separating the parent metals and form sound metallurgical interface at either side. For example, Yang et al. [10] successfully obtained laser welded/brazed Al/steel dissimilar joint by using an Al–Si filler metal. Chen et al. [11] fabricated laser welded/brazed Al/Ti joint with an Al–Si filler metal. By inserting an AZ31B filler metal, Tan et al. [12] performed laser welding/brazing of Mg to steel joint. While, no successful study has been reported on Al/Mg joint by laser welding/brazing technology, which may be attributed to the small difference in melting point between Al and Mg base metals. Despite this problem, laser welding/brazing could be still realised by inserting an appropriate interlayer to create great

CONTACT Jin Yang jyang@sues.edu.cn School of Materials Engineering, Shanghai University of Engineering Science, Shanghai, 201620, People's Republic of China

melting point differences between Al/interlayer and interlayer/Mg. With this in mind, it is hypothetic that Ni interlayer, with its high melting point characteristic and good metallurgical capability with Al and Mg, could be a promising candidate. In fact, Ni interlayer has been used for Al/Mg dissimilar joining in many welding processes, for example, resistance spot welding [13], friction stir welding [14] and laser keyhole welding [15]. However, the investigation on laser welding/brazing of Al to Mg using Ni interlayer is still lacking. Therefore, the aim of this study is to investigate the feasibility of laser welding/brazing of Al to Mg via Ni interlayer. The influence of Ni interlayer on the interfacial microstructure and joint strength was discussed by comparing the laser joints obtained with and without Ni interlayer. The results have shown that a reliable laser welded/brazed Al/Mg joint is successfully achieved via a Ni interlayer. Owing to the presence of Ni interlayer, the joint strength is significantly enhanced.

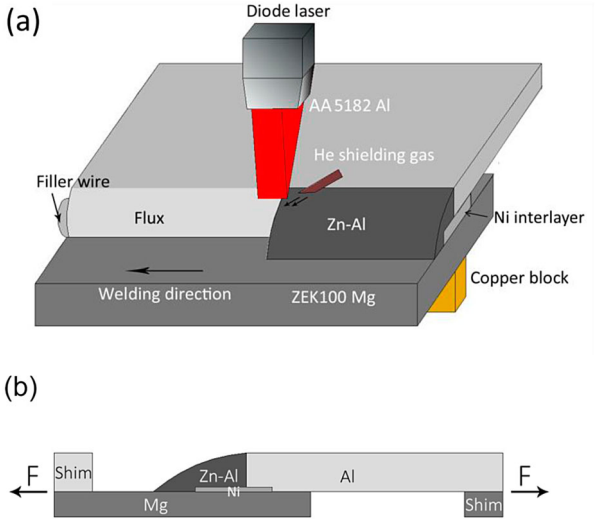

Figure 1. (a) Schematic description of the experimental layout used for laser welding/brazing of aluminium to magnesium with Ni interlayer. (b) Schematic description of the tensile-shear test samples.

Experimental procedures

AA5182 Al alloy and ZEK100 Mg alloy sheets were used for the present study. The sheets were cut into 50 mm × 60 mm × 1.5 mm specimens. $ZnAl_{22}$ filler metal with the diameter of 1.6 mm was used. Chemical compositions and mechanical properties of the materials are given in Tables 1 and 2 [16]. Ni interlayer (99.9 wt-% pure) in the dimension of 60 mm × 10 mm × 0.2 mm was used. The commercial flux used in the experiments was Superior No. 21 manufactured by Superior Flux and Mfg. Co. This powder flux was composed of LiCl (35–40 wt-%), KCl (30–35 wt-%), NaF (10–25 wt-%), NaCl (8–13 wt-%), and ZnCl2 (6–10 wt-%).

Figure 1(a) shows the schematic of laser welding/brazing process. An integrated Panasonic 6-axis robot and Nuvonyx diode laser system with a maximum power of 4.0 kW and a 1 mm × 12 mm rectangular laser beam intensity profile at the focal point was used for laser welding/brazing. This energy distribution is more suitable for laser welding/brazing processes compared with the non-uniform Gaussian-distributed circular beams. To remove oil and oxides of surface of coupons, the coupons went through a very strict two-step cleaning process. The first step was that the surfaces of all the coupons were ultrasonically cleaned in ethanol for 10 min. The second step was that the surfaces of the Al coupons were cleaned with a solution of 1.2 ml HF, 67.5 ml HNO_3 and 100 ml water, while the surfaces of Mg coupons were cleaned with a solution of 2.5 g chromic oxide and 100 ml water. The as-received powder flux was mixed with ethanol into a paste and then evenly sprinkled on the sample to obtain an estimated average thickness of 10–50 μm. The lap joint configuration was made by placing Al sheet on top of Mg sheet with the Ni interlayer in-between. The filler metal was preset on the surface of Ni interlayer. Helium shielding gas was provided with a flow rate of 15 l min^{-1} to limit oxidation. The process parameters were 1.8–2.6 kW laser power, 0.15–0.30 m min^{-1} travel speed, and the laser beam was focused on top of the filler metal.

After welding, cross-sections of the laser joint were cut, and then mounted in phenolic resin. The samples were mechanically ground using 400, 600, 800, 1000 and 1200 grade SiC abrasive papers followed by polishing with a 1-μm diamond suspension. To analyse the microstructure and determine the chemical composition of the interfacial phases, the cross-sections were observed using Olympus BX51M optical microscope and Zeiss Leo 1530 scanning electron microscope (SEM) equipped with EDAX Genesis energy-dispersive X-ray spectroscopy (EDS) analysis. The phase constitution of fractured joints was analysed by X-ray diffraction (XRD) using an INEL XRG-3000 diffractometer with Cu Kα1 radiation (wavelength $\lambda = 1.5406$ Å) at 30 kV and 30 mA.

Tensile test specimens were cut from the laser joints by abrasive water jet. The specimens were subjected to

Table 1. Chemical composition of the materials in wt-%.

Materials	Mg	Cr	Mn	Si	Cu	Zn	Ti	Fe	Zr	Ce	Al
AA 5182 Al	–	0.15	2.1	0.2	0.15	0.25	0.1	0.35	< 0.01		Bal.
ZEK100 Mg	Bal.	–	–	–	–	1.3	–	–	0.5	0.2	–
$ZnAl_{22}$	–	–	–	–	–	Bal.	–	–	–	–	22.0

Table 2. Mechanical properties of the base materials [13].

Materials	Yield strength (MPa)	Ultimate strength (MPa)	Elongation (%)
ZEK100 Mg	305 ± 3	313 ± 3	7.5 ± 0.1
AA 5182 Al	138 ± 11	275 ± 3	25 ± 1.3

uniaxial tensile-shear tests at room temperature, performed with a crosshead speed of 1 mm min^{-1} using an Instron 5548 Micro Tester, and the loading direction was perpendicular to the joining line, as shown in Figure 1(b). Shims were used at each end of the specimens to ensure that bending loads were minimised.

Results and discussion

Microstructure

Figure 2(a) presents the cross-section of a typical laser welded Al/Mg joint without Ni interlayer at 2.2 kW laser power and 0.2 m min^{-1} travel speed. As shown, lots of porosities are observed at the lower part of fusion zone (FZ). Besides, fractures and cracks are obvious in the FZ. Figure 2(b) shows the higher magnification in the highlighted square in Figure 2(a). Similar microstructure is observed on both sides of the fracture. The backscattering electron image shows that the microstructure is composed of grey dendrites and light lamellar structures in the inter-dendrite regions. By close observation at the inset, it is evident that the fracture is prone to bypass the dendrites and only propagate along the light lamellar structures. Based on the EDS analysis (Table 2) and Al–Mg–Zn ternary phase diagram [17], the possible phases of grey dendrites and lamellar structures are Al solid solution as well as Al solid solution and $MgZn_2$ IMCs, respectively. Li et al. [18] reported that $MgZn_2$ is a hard and brittle phase in the study of laser welding/brazing of Mg to steel. Thus, the fracture would prefer to form and propagate in $MgZn_2$.

Figure 3(a) presents the cross-section of a typical laser welded/brazed Al/Mg joint with Ni interlayer at 2.2 kW laser power and 0.2 m min^{-1} travel speed. Comparing to Figure 2(a), the amount of porosity is markedly reduced. Besides, fracture and crack can be hardly observed in the joint. The origin of the difference will be discussed later.

During laser irradiation, Zn–Al filler metal and part of Al and Mg base metals melted while Ni interlayer stayed unmelt owing to differences in the melting point. Consequently, two pairs of welded/brazed interfaces are formed in the joint. One pair is the Zn–Al FZ/Al-based metal welded interface and Zn–Al FZ/Ni brazed interface, which are above the Ni interlayer. The other pair is Mg FZ/Mg base metal welded interface and Ni/Mg FZ brazed interface, which are below the Ni interlayer. The interfaces are sequentially marked as A, B, C and D. Figure 3(b) shows the magnified image at zone A, primary α-Al dendrites as well as eutectoid α-Al and β-Zn at inter-dendrite region are observed near the Zn–Al FZ/Al welded interface. At zone B, the Zn–Al FZ/Ni brazed interface, a wavy reaction layer was formed, as illustrated in Figure 3(c). Based on the EDS analysis (Table 3) and Zn–Ni binary phase diagram [19], the possible phase was Ni_5Zn_{21}. Figure 3(d) shows the magnified image at zone C, distinct reaction products are obvious at Ni/Mg FZ brazed interface. The backscattering electron image shows that the reaction layer is composed of a grey layer, a lamellar structure and dispersed light particles. According to the EDS analysis, the possible phases of the grey structure, lamellar structure and light particles are $MgNi_2$, eutectic α-Mg and Mg_2Ni, and AlNi (Table 3). The phases were confirmed by XRD analysis as will be shown later. At zone D, the interface between Mg FZ and Mg base metal is also well welded, which is composed of primary α-Mg dendrites, AlNi particles and eutectic α-Mg and Mg_2Ni.

Mechanical properties and fractography

Owing to the non-symmetric configuration of the tensile-shear test specimens (Figure 1(b)), a combination of shear and tensile forces exist at the interface. Consequently, the joint strength is reported here as fracture load, since it is not possible to separate tensile and shear stresses. Table 4 presents strength of laser joints with and without Ni interlayer. As

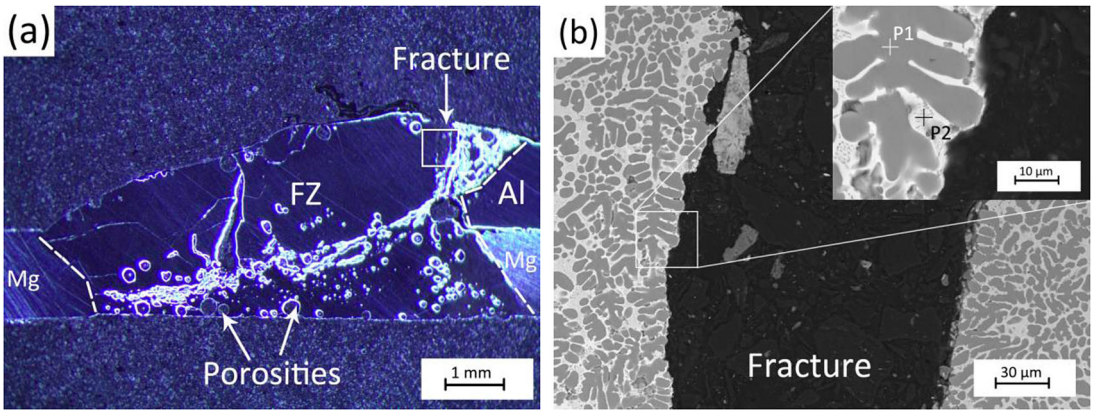

Figure 2. (a) Optical image of cross-section of laser Al/Mg joint without Ni interlayer at 2.2 kW laser power and 0.2 m min^{-1} travel speed. (b) SEM image of highlighted square in (a). Inset is the enlarged view of the square in (b).

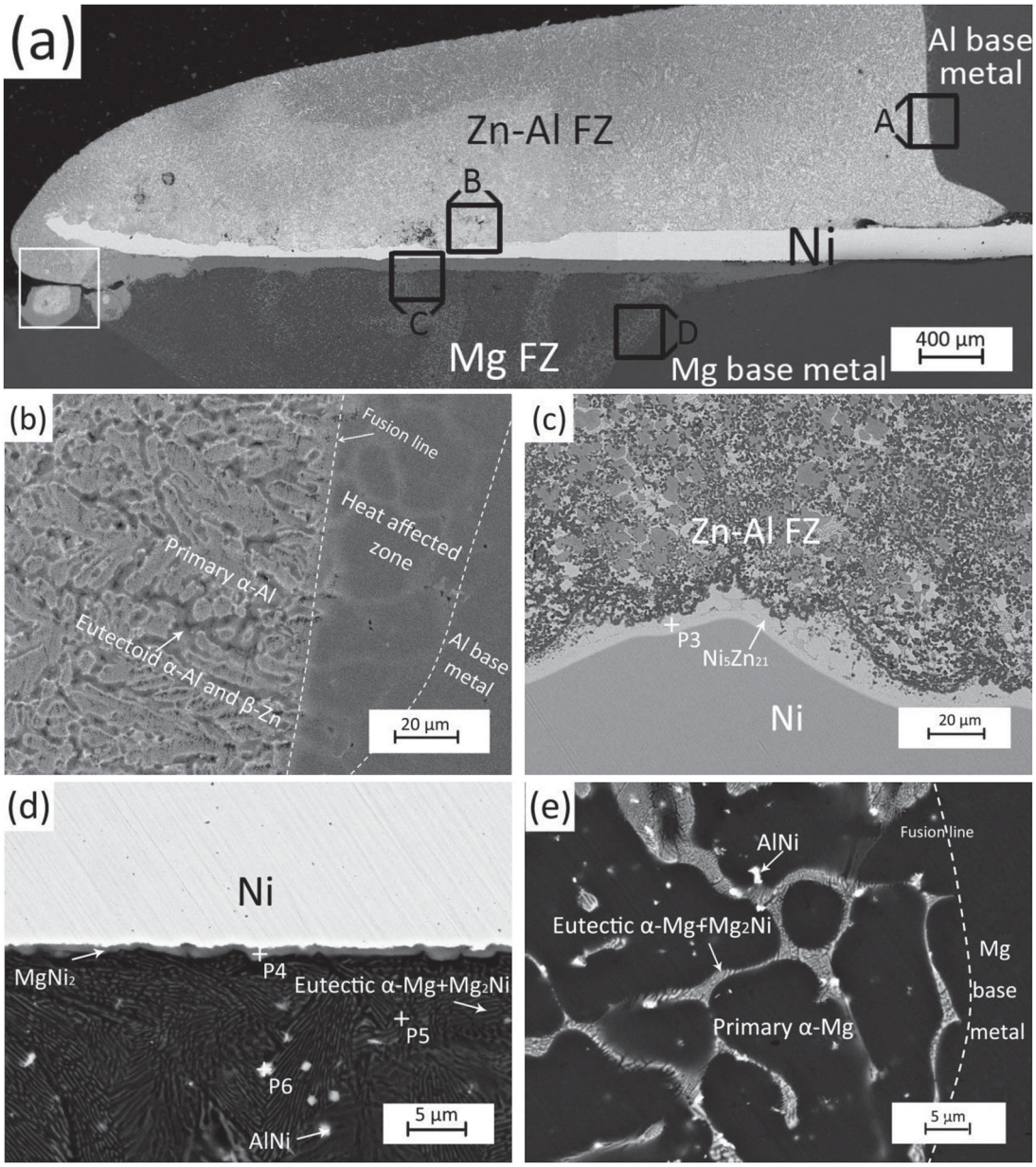

Figure 3. (a) Overall view of cross-section of laser Al/Mg joint with Ni interlayer at 2.2 kW laser power and 0.2 m min^{-1} travel speed, (b) zone A, (c) zone B, (d) zone C and (e) zone D.

Table 3. EDS analysis of the marked zones in Figs. 2(b), 3(c) and 3(d) in at.-%.

No.	Mg	Al	Zn	Ni	Possible phases
P1	3.8 ± 0.9	89.1 ± 2.3	7.2 ± 0.6	–	Al solid solution
P2	21.9 ± 2.9	43.3 ± 5.2	34.8 ± 2.2	–	Al solid solution + $MgZn_2$
P3	–	5.2 ± 0.5	73.7 ± 1.3	21.1 ± 0.8	Ni_5Zn_{21}
P4	12.0 ± 1.2		–	88.0 ± 3.7	$MgNi_2$
P5	88.9 ± 0.8		1.0 ± 0.2	9.1 ± 0.6	α-Mg + Mg_2Ni
P6	6.1 ± 1.8	49.9 ± 3.0	–	44.0 ± 3.1	AlNi

shown, the strength of laser joint without Ni interlayer is zero. The tensile testing coupons fracture either during coupon processing or after coupon clamping in tensile tests. This is mainly owing to the preformed porosities, cracks and fractures in the joint (Figure 2(a)). However, the joint strength increases to 410 ± 25 N with the Ni interlayer. This enhancement in joint strength is apparently owing to the formation of metallurgical bonding between the interfaces (Figure 3).

Table 4. Joint strength of dissimilar laser Mg/Al joints.

	With Ni	Without Ni
Joint strength (N)	410 ± 25	0

Figure 4 displays the SEM and EDS analyses of fracture surface of the joint with Ni interlayer. The fracture surface on the Ni side exhibited rugged structures with some tortuous facets, which was an indication of plastic deformation (Figure 4(a)). The fracture surface on the

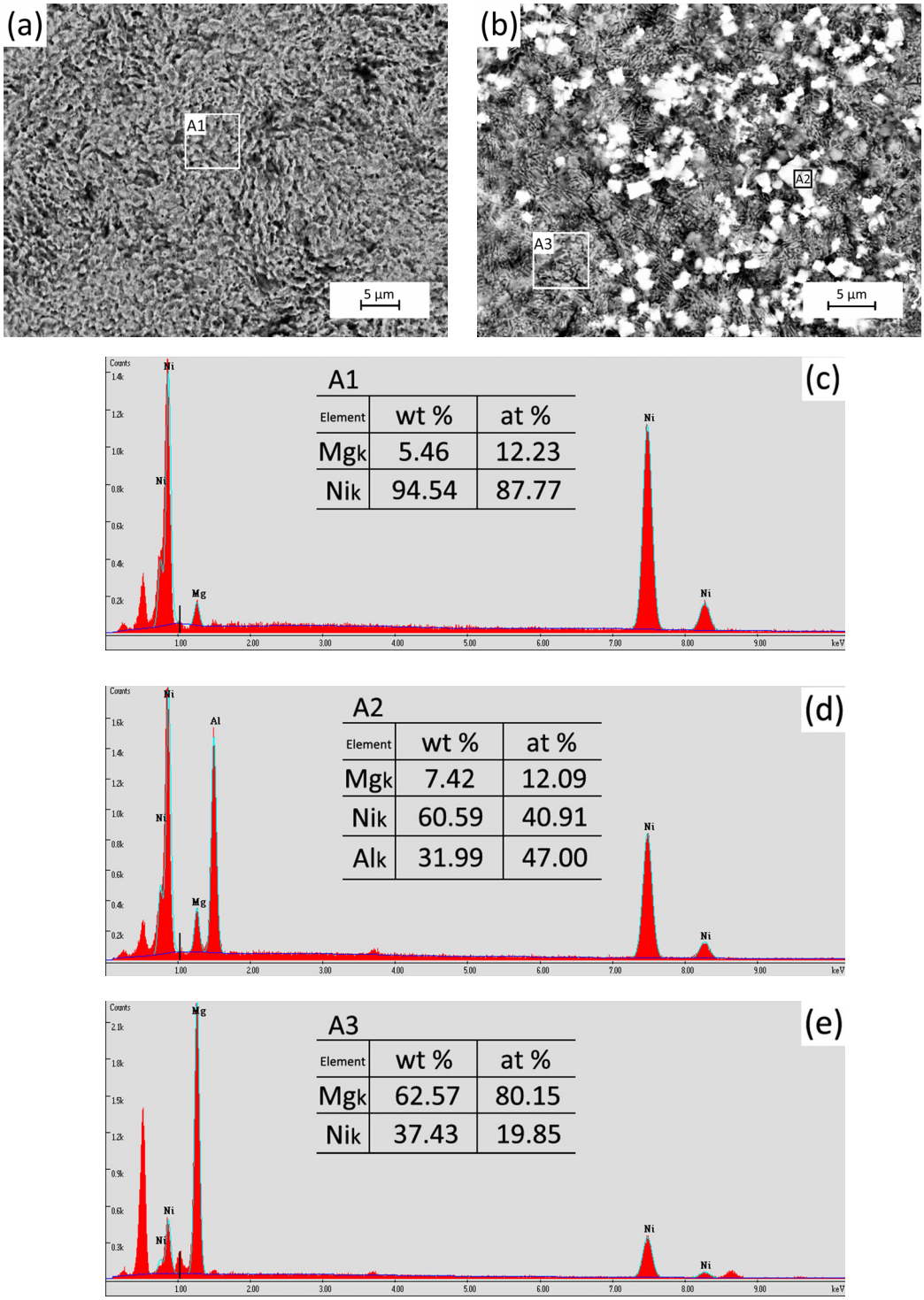

Figure 4. SEM and EDS analysis on the fracture surfaces: (a–b) SEM analysis on the fracture surface at Ni side and Mg side, respectively, and (c–e) EDS analysis on fracture surface at A1-A3 in (a–b).

Mg side displayed lamellar structures with some light particles on top, and no apparent indication of plastic deformation was observed (Figure 4(b)). Figure 4(c–e) shows the EDS analysis results. At Ni side, the elemental ratio of Mg to Ni is around 1:7, which could be $MgNi_2$ (Figure 4(c)). At Mg side, the light particle structure has the 1:1 Al to Ni elemental ratio, which corresponds to the stoichiometry of AlNi (Figure 4(d)); while, the elemental ratio of Mg to Ni for lamellar structure is around 4:1, which is probably α-Mg and Mg_2Ni (Figure 4(e)). All the phases are then confirmed by XRD analysis in Figure 5(a,b). As shown, peaks of $MgNi_2$ are presented at Ni side, and peaks of Mg_2Ni and AlNi are shown at Mg side. Thus, it is suggested that the fracture occurred at the interface between Mg_2Ni and $MgNi_2$. Note that peaks of Mg_2Al_3 were identified in the XRD analysis. Formation of Mg_2Al_3 is expected to be induced by the direct metallurgical reaction between Mg and Al at the weld toe as indicated in Figure 3(a) by a white square. A further study is needed to investigate

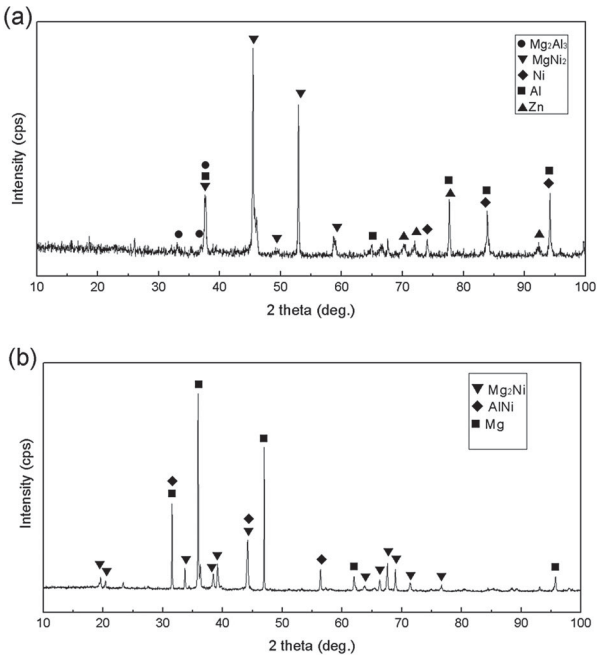

Figure 5. XRD patterns on the fracture surfaces: (a) Ni side and (b) Mg side.

the influence of Mg_2Al_3 on the joint mechanical properties.

Influence of Ni interlayer

During laser welding/brazing process, the Ni interlayer with a melting point of 1453°C would not melt, while Zn–Al filler metal (melting point 482°C) and a part of Al and Mg base metal (melting points 640°C approximately) would melt. With this in mind, the role of the Ni interlayer in dissimilar joining of Al and Mg could be divided into two parts. The first was acting as a thermal barrier. Comparing Figure 2(a) to Figure 3(a), the porosities induced by the evaporation of Mg were remarkably reduced. This could be because Ni interlayer absorbed a certain amount of laser heat input and effectively decreased the temperature in the Mg base metal. The second was served as a diffusion barrier to produce preferable reaction products as will be discussed in the section 'Formation of interfacial phases and joining mechanism' below, which enhanced the joint strength (Table 4).

Formation of interfacial phases and joining mechanism

To the best knowledge of the authors, Al alloy and Mg alloy are, for the first time, successfully joined by using laser welding/brazing technology in the help of a Ni interlayer. Note that the distinctively uniform thermal distribution provided by diode laser is a very important factor for the realisation of this technology. Besides, the resultant two pairs of welded/brazed interfaces, i.e. Zn–Al FZ/Al and Mg FZ/Mg welded interfaces as well

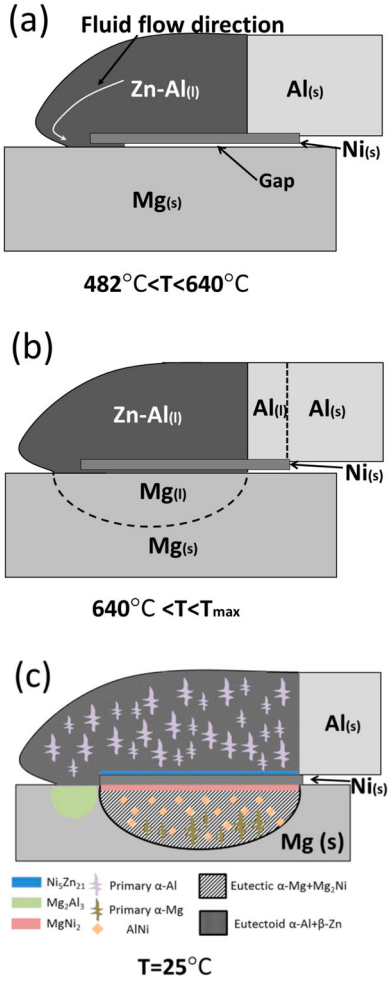

Figure 6. Joint formation during laser welding/brazing of Al to Mg with Ni interlayer: (a) wetting of Ni interlayer by molten Zn–Al filler metal and flowing of the filler metal into the gap between Mg and Ni, (b) phase transformation of Al and Mg base metals and (c) formation of the phases and joint.

as Zn–Al FZ/Ni and Ni/Mg FZ brazed interfaces, are also very crucial, which are responsible for the joint formation. Thus, it is of importance to discuss formation mechanism of the laser joint. A schematic illustration is provided to assist the following discussion.

First, when the temperature rose above the melting point of the Zn–Al filler metal, the filler metal began to melt and started to wet on the Ni interlayer and also flowed into the gap between Ni and Mg because of the capillary action (Figure 6(a)). The gap was believed to be caused by the difference of base metals' surface asperity at the faying surface. Second, as the temperature continued to increase, a part of the Al base metal and Mg substrate melted forming fusion zones (Figure 6(b)). Thirdly, different physical and chemical processes occurred at the interfaces (Figure 6(c)). At the Zn–Al FZ/Al welded interface, primary α-Al dendrites as well as eutectoid α-Al and β-Zn at interdendrite region nucleated upon cooling. At the Zn–Al FZ/Ni brazed interface, Ni_5Zn_{21} was formed because of diffusion-controlled reactions between solid Ni and molten Zn–Al [20]. At the Ni/Mg FZ brazed interface,

planar $MgNi_2$ and eutectic α-Mg and Mg_2Ni were expected to be caused by the diffusion-controlled reaction mechanism, while dispersed AlNi particles might be formed by the precipitation mechanism [13,21]. At the Mg FZ/Mg welded interface, nucleation occurred in the mixed molten pool consisting of Zn–Al, Mg and dissolved Ni, which led to the formation of primary α-Mg dendrites, AlNi particles and eutectic α-Mg and Mg_2Ni [15]. At the weld toe, owing to the direct mixing of Zn–Al and Mg, tiny amount of Mg_2Al_3 was formed.

Conclusions

Dissimilar joining of 5182 aluminium alloy to ZEK100 magnesium alloy was achieved successfully by laser welding/brazing technology using a nickel interlayer. The microstructure, joint mechanical properties and fracture behaviour were investigated. Besides, the influence of Ni interlayer was studied by comparing the joints obtained with and without Ni interlayer. The major conclusions can be summarised as follows:

(1) Two pairs of welded/brazed interfaces are observed in the dissimilar laser Al/Mg joint. One pair is above the Ni interlayer: at the Zn–Al FZ/Al welded interface, primary α-Al as well as eutectoid α-Al and β-Zn are nucleated; at the Zn–Al FZ/Ni brazed interface, a layer of Ni_5Zn_{21} is generated. While, the other pair is below the Ni interlayer: at the Ni/Mg FZ brazed interface, planar $MgNi_2$, AlNi particles and eutectic α-Mg and Mg_2Ni are produced, at the Mg FZ/Mg welded interface, primary α-Mg, AlNi particles and eutectic α-Mg and Mg_2Ni are formed.
(2) By inserting the Ni interlayer, the joint strength increases from 0 to 410 N. The fracture occurs at the Ni/Mg FZ brazed interface.
(3) The Ni interlayer plays a dual role in laser welding/brazing of Al to Mg, including thermal and diffusion barriers. As a result, the amount of Mg porosities is significantly reduced owing to the role of thermal barrier, and the microstructure is altered owing to the role of diffusion barrier, which induces the joint strength enhancement.

Disclosure statement

No potential conflict of interest was reported by the authors.

Funding

This work was supported by National Natural Science Foundation of China (grant numbers 51375294 and 51665038) and NSERC is gratefully acknowledged.

ORCID

Jin Yang http://orcid.org/0000-0001-5226-4815

References

[1] Chowdhury SH, Chen DL, Bhole SD, et al. Lap shear strength and fatigue behavior of friction stir spot welded dissimilar magnesium-to-aluminium joints with adhesive. Mater Sci Eng A. 2013;562(1):53–60.
[2] Sato YS, Park SHC, Michiuchi M, et al. Constitutional liquation during dissimilar friction stir welding of Al and Mg alloys. Scripta Mater. 2004;50(9):1233–1236.
[3] Choi DH, Ahn BW, Lee CY, et al. Formation of intermetallic compounds in Al and Mg alloy interface during friction stir spot welding. Intermetallics. 2011;19(2):125–130.
[4] Liu L, Ren D, Liu F. A review of dissimilar welding techniques for magnesium alloys to aluminum alloys. Materials. 2014;7(5):3735–3757.
[5] Scherm F, Bezold J, Glatzel U. Laser welding of Mg alloy MgAl3Zn1 (AZ31) to Al alloy AlMg3 (AA5754) using ZnAl filler material. Sci Technol Weld Join. 2012;17(5):364–367.
[6] Penner P, Liu L, Gerlich A, et al. Dissimilar resistance spot welding of aluminum to magnesium with Zn-coated steel interlayers. Weld J. 2014;93(6):225S–231S.
[7] Firouzdor V, Kou S. Al-to-Mg friction stir welding: effect of material position, travel speed, and rotation speed. Mater Trans A. 2010;41(11):2914–2935.
[8] Panteli A, Chen YC, Strong D, et al. Optimization of aluminium-to-magnesium ultrasonic spot welding. JOM. 2012;64(3):414–420.
[9] Patel VK, Bhole SD, Chen DL. Microstructure and mechanical properties of dissimilar welded Mg–Al joints by ultrasonic spot welding technique. Sci Technol Weld Join. 2013;17(3):202–206.
[10] Yang J, Li Y, Zhang H, et al. Dissimilar laser welding/brazing of 5754 aluminum alloy to DP 980 steel: mechanical properties and interfacial microstructure. Metall Mater Trans A. 2015;46(11):5149–5157.
[11] Chen S, Zhai Z, Huang J, et al. Interface microstructure and fracture behavior of single/dual-beam laser welded steel-Al dissimilar joint produced with copper interlayer. Int J Min Met Mater. 2016;82(1):631–643.
[12] Tan C, Song X, Meng S, et al. Laser welding-brazing of Mg to stainless steel: joining characteristics, interfacial microstructure, and mechanical properties. Int J Adv Manuf Tech. 2016;86(1):1–11.
[13] Sun M, Niknejad ST, Zhang G, et al. Microstructure and mechanical properties of resistance spot welded AZ31/AA5754 using a nickel interlayer. Mater Des. 2015;87:905–913.
[14] Chang WS, Rajesh SR, Chun CK, et al. Microstructure and mechanical properties of hybrid laser-friction stir welding between AA6061-T6 Al alloy and AZ31 Mg alloy. J Mater Sci Technol. 2011;27(3):199–204.
[15] Wang H, Liu L, Liu F. The characterization investigation of laser-arc-adhesive hybrid welding of Mg to Al joint using Ni interlayer. Mater Des. 2013;50(17):463–466.
[16] ASM Handbook Vol. 2, Properties and Selection: Nonferrous Alloys and Special-Purpose Materials, Materials Park, OH: ASM Int'l, 1993.
[17] Raghavan V. Al-Mg-Zn (Aluminum-Magnesium-Zinc). J Phase Equilib Diff. 2010;31(3):293–294.
[18] Li L, Tan C, Chen Y, et al. Influence of Zn coating on interfacial reactions and mechanical properties during laser welding-brazing of Mg to steel. Metall Mater Trans A. 2012;43(12):4740–4754.
[19] Okamoto H. Ni-Zn (Nickel-Zinc). J Phase Equilib Diff. 2013;34(2):153–153.

[20] Wang CH, Chen HH, Li PY, et al. Kinetic analysis of Ni_5Zn_{21}, growth at the interface between Sn-Zn solders and Ni. Intermetallics. 2012;22(3): 166–175.

[21] Penner P, Liu L, Gerlich A, et al. Feasibility study of resistance spot welding of dissimilar Al/Mg combinations with Ni based interlayers. Sci Technol Weld Join. 2013;18(7):541–550.